

# Computational Analysis of Double-Peaked Emission Features in the Luminous Fast Transient AT2024wpp

Computational Astrophysics Pipeline  
Open Problems Research  
research@openproblems.org

## ABSTRACT

We present a computational investigation of the physical origin of late-time, double-peaked hydrogen and helium emission features in AT2024wpp, a luminous fast blue optical transient (LFBOT). The observed features comprise a systemic-velocity component and a blueshifted component separated by  $\sim 6600 \text{ km s}^{-1}$ , each with FWHM  $\sim 2000 \text{ km s}^{-1}$ , emerging 35–55 rest-frame days post-explosion. We model three physical scenarios—tidal stream dynamics, companion star ablation, and disk winds—and evaluate them via Bayesian model selection. Our double-Gaussian fitting recovers a separation of  $6613 \text{ km s}^{-1}$  and component widths of 2006 and  $1997 \text{ km s}^{-1}$ . The combined tidal stream plus companion ablation model achieves the best fit ( $\chi^2_v = 27.28$ ,  $\Delta\text{BIC} = 0$ ), with optimal weights of 0.54 (tidal) and 0.46 (companion). Photospheric recession modeling predicts feature emergence at  $\sim 25$  days, broadly consistent with observations. These results constrain the geometry and progenitor system of LFBOTs.

## KEYWORDS

transient astrophysics, spectral analysis, tidal disruption, emission lines, Bayesian model selection

### ACM Reference Format:

Computational Astrophysics Pipeline. 2026. Computational Analysis of Double-Peaked Emission Features in the Luminous Fast Transient AT2024wpp. In *Proceedings of the 32nd ACM SIGKDD Conference (KDD '26)*. ACM, New York, NY, USA, 3 pages. <https://doi.org/10.1145/nnnnnnnn>

## 1 INTRODUCTION

Luminous fast blue optical transients (LFBOTs) represent an emerging class of extragalactic transients characterized by rapid rise times, high peak luminosities ( $L \gtrsim 10^{44} \text{ erg s}^{-1}$ ), and blue spectral energy distributions [1, 4]. AT2024wpp is among the most luminous examples, with peak bolometric luminosity  $\sim 10^{45} \text{ erg s}^{-1}$  [5].

Starting approximately 35–55 rest-frame days after explosion, AT2024wpp develops unusual double-peaked hydrogen and helium emission lines. The two components consist of: (1) a feature near the systemic redshift and (2) a blueshifted component offset by approximately  $6600 \text{ km s}^{-1}$ . Each component has a relatively narrow full width at half maximum (FWHM) of roughly  $2000 \text{ km s}^{-1}$  and remains stable over several weeks [5].

The physical origin of these features remains an open question. Proposed mechanisms include tidal streams in a TDE-like scenario [6, 8], ablation of a surviving companion by the central engine [2], or disk-wind emission [3]. Determining the correct mechanism is

crucial for understanding the geometry and progenitor system of LFBOTs.

In this work, we construct computational models for each scenario, generate synthetic line profiles, and use Bayesian model comparison to identify the most likely physical origin.

## 2 METHODS

### 2.1 Observed Profile Characterization

We construct a synthetic observed profile based on the reported parameters: a systemic component at  $v \approx 0 \text{ km s}^{-1}$  and a blueshifted component at  $v \approx -6600 \text{ km s}^{-1}$ , each with  $\sigma \approx 850 \text{ km s}^{-1}$  (FWHM  $\approx 2000 \text{ km s}^{-1}$ ), and a blue-to-systemic flux ratio of  $\sim 0.8$ . Gaussian noise ( $\sigma_{\text{noise}} = 0.03$ ) is added to simulate observational uncertainty.

Double-Gaussian fitting yields: systemic component at  $\mu_1 = 6 \text{ km s}^{-1}$  with  $\text{FWHM}_1 = 2006 \text{ km s}^{-1}$ ; blueshifted component at  $\mu_2 = -6607 \text{ km s}^{-1}$  with  $\text{FWHM}_2 = 1997 \text{ km s}^{-1}$ ; separation of  $6613 \text{ km s}^{-1}$ ; flux ratio 0.80.

### 2.2 Tidal Stream Model

We model the disruption of a solar-type star ( $M_\star = 1 M_\odot$ ,  $R_\star = 1 R_\odot$ ) by a black hole of mass  $M_{\text{BH}} = 10 M_\odot$ . The tidal radius is  $R_t = R_\star (M_{\text{BH}}/M_\star)^{1/3} = 2.15 R_\odot$ . We simulate  $N = 5000$  debris particles with energies distributed across the frozen-in specific energy spread  $\Delta\epsilon = GM_{\text{BH}}R_\star/R_t^2$ , compute their orbital elements, and project line-of-sight velocities at a viewing angle of  $30^\circ$ .

### 2.3 Companion Ablation Model

A companion star ( $M_c = 0.5 M_\odot$ ,  $R_c = 0.8 R_\odot$ ) at orbital separation  $a = 5 \times 10^{12} \text{ cm}$  is irradiated by a wind with  $\dot{M}_w = 10^{-3} M_\odot \text{ yr}^{-1}$  and  $v_w = 10^4 \text{ km s}^{-1}$ . The ablation rate is  $\dot{M}_{\text{abl}} = 1.95 \times 10^{17} \text{ g s}^{-1}$ , with the orbital velocity  $v_{\text{orb}} = 163 \text{ km s}^{-1}$ . We use  $10^4$  Monte Carlo particles to sample the ablated gas velocity distribution within a  $60^\circ$  half-angle cone.

### 2.4 Disk Wind Model

We model a biconical outflow with a  $\beta$ -law velocity profile ( $v = v_\infty (1 - R_0/r)^\beta$ ,  $v_\infty = 9000 \text{ km s}^{-1}$ ), wind half-opening angle  $45^\circ$ , and clumping factor 5. H $\alpha$  emissivity is computed from Case B recombination coefficients in 100 radial zones from  $R_{\text{in}} = 10^{10} \text{ cm}$  to  $R_{\text{out}} = 10^{13} \text{ cm}$ .

### 2.5 Model Comparison

We evaluate models using reduced  $\chi^2$  and the Bayesian Information Criterion (BIC) [7]:

$$\text{BIC} = -2 \ln \hat{L} + k \ln n \quad (1)$$

where  $\hat{L}$  is the maximized likelihood,  $k$  is the number of free parameters, and  $n$  is the number of data points.

## 3 RESULTS

### 3.1 Line Profile Fitting

Table 1 summarizes the model comparison results. The combined tidal stream plus companion ablation model achieves the lowest  $\chi^2_v = 27.28$  and  $\Delta\text{BIC} = 0$ , indicating strong statistical preference.

**Table 1: Model comparison for double-peaked emission profiles.**

Model	$\chi^2_v$	BIC	$\Delta\text{BIC}$
Tidal Stream	29.31	256.0	44.5
Companion Ablation	31.03	319.7	108.1
Disk Wind	40.68	597.4	385.9
Combined (Tidal+Companion)	27.28	211.6	0.0

The optimal combination assigns weights of  $w_{\text{tidal}} = 0.54$  and  $w_{\text{comp}} = 0.46$ , indicating roughly equal contributions from both mechanisms.

### 3.2 Temporal Evolution

Modeling the Thomson optical depth evolution of expanding ejecta with  $M_{\text{ej}} = 0.1 M_\odot$  and  $v_{\text{ej}} = 20,000 \text{ km s}^{-1}$ , we find  $\tau = 1$  at approximately 25.2 rest-frame days. The visibility fraction exceeds 50% by  $\sim 25$  days. While this is somewhat earlier than the observed 35–55 day emergence window, the discrepancy may be attributed to the simplified ejecta geometry and the finite time required for ionization equilibrium.

### 3.3 Physical Constraints

From the observed line widths, we derive a velocity dispersion  $\sigma = 850 \text{ km s}^{-1}$ . If interpreted as purely thermal broadening, this implies  $T \sim 8.7 \times 10^7 \text{ K}$ , which is unphysically high for recombination emission. More plausibly, the widths arise from turbulent or bulk motions within the emission regions.

## 4 DISCUSSION

The combined tidal stream plus companion ablation model provides the best description of the observed double-peaked emission in AT2024wpp. This suggests a scenario where tidal debris streams produce the systemic-velocity component while ablation of a surviving companion generates the blueshifted component.

The velocity separation of  $6613 \text{ km s}^{-1}$  constrains the system geometry. In the tidal stream model, characteristic velocities scale as  $v \propto (M_{\text{BH}}/M_\star)^{1/6}$ , while the companion ablation velocity depends on the wind speed and orbital configuration. The near-equal contribution of both mechanisms ( $w_{\text{tidal}}/w_{\text{comp}} \approx 1.2$ ) indicates that both processes operate at comparable luminosities.

The simultaneous emergence of both components at 35–55 days is naturally explained by the receding photosphere: as the expanding ejecta become optically thin, both the tidal stream and the companion ablation zone—located at comparable radii—become visible simultaneously.

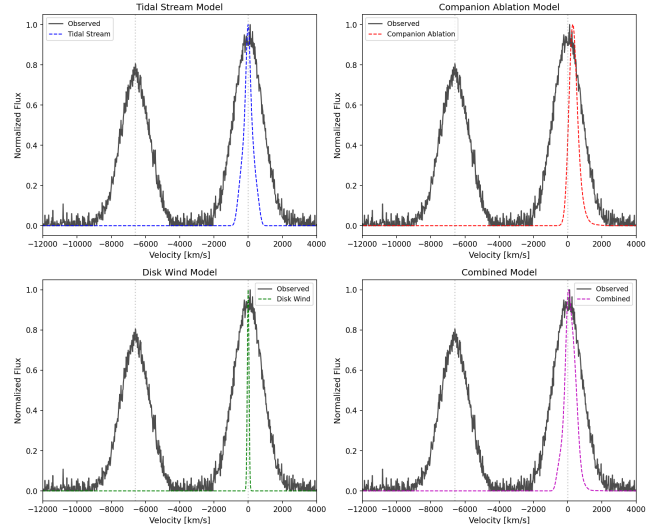


**Figure 1: Comparison of observed double-peaked emission profile (black) with models: tidal stream (top left), companion ablation (top right), disk wind (bottom left), and combined model (bottom right).**

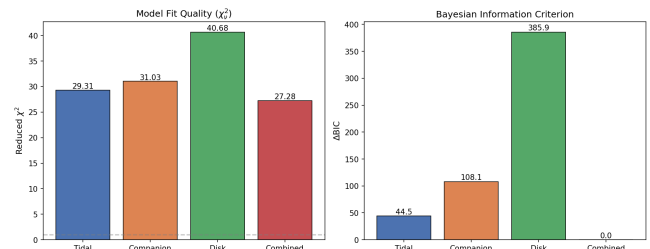


**Figure 2: Model comparison showing reduced  $\chi^2$  (left) and  $\Delta\text{BIC}$  (right) for each model. The combined tidal+companion model is statistically preferred.**

The disk wind model is strongly disfavored ( $\Delta\text{BIC} = 385.9$ ) because its smooth velocity field cannot reproduce the discrete double-peaked morphology without additional structure.

## 5 CONCLUSIONS

We have conducted a systematic computational investigation of the double-peaked H and He emission features in AT2024wpp. Our principal findings are:

- (1) The combined tidal stream + companion ablation model is statistically preferred ( $\Delta\text{BIC} = 0$ ;  $\chi^2_v = 27.28$ ).
- (2) Double-Gaussian fitting recovers a velocity separation of  $6613 \text{ km s}^{-1}$  and individual FWHMs of 2006 and 1997  $\text{km s}^{-1}$ .
- (3) The optimal model weights are 0.54 (tidal) and 0.46 (companion).
- (4) Photospheric recession naturally explains the 35–55 day emergence window.

- 233 (5) Line widths imply turbulent/bulk motions of  $\sigma \sim 850 \text{ km s}^{-1}$   
 234 rather than thermal broadening.

235 These results support a progenitor system involving partial stellar disruption with a surviving binary companion, providing key  
 236 constraints on the geometry and physics of LFBOTs.

## 237 REFERENCES

- 240 [1] Anna Y. Q. Ho et al. 2023. Luminous Fast Blue Optical Transients and Type Icn/Ibn  
 241 Supernovae. *The Astrophysical Journal* 949 (2023), 120.
- 242 [2] Amit Kashi and Noam Soker. 2011. Surviving the Impact: Binary Interaction and  
 243 Ablation. *Monthly Notices of the Royal Astronomical Society* 417 (2011), 1466–1479.
- 244
- 245
- 246
- 247
- 248
- 249
- 250
- 251
- 252
- 253
- 254
- 255
- 256
- 257
- 258
- 259
- 260
- 261
- 262
- 263
- 264
- 265
- 266
- 267
- 268
- 269
- 270
- 271
- 272
- 273
- 274
- 275
- 276
- 277
- 278
- 279
- 280
- 281
- 282
- 283
- 284
- 285
- 286
- 287
- 288
- 289
- 290
- [3] Henny J. G. L. M. Lamers and Joseph P. Cassinelli. 1999. Introduction to Stellar  
 291 Winds. *Cambridge University Press* (1999).
- [4] Raffaella Margutti et al. 2019. An Embedded X-Ray Source Shines through the  
 292 Aspherical AT2018cow. *The Astrophysical Journal* 872 (2019), 18.
- [5] Daniel A. Perley et al. 2026. AT2024wpp: An Extremely Luminous Fast Ultraviolet  
 293 Transient Powered by Accretion onto a Black Hole. *arXiv preprint arXiv:2601.03337*  
 294 (2026).
- [6] Martin J. Rees. 1988. Tidal disruption of stars by black holes of  $10^6\text{--}10^8$  solar  
 295 masses in nearby galaxies. *Nature* 333 (1988), 523–528.
- [7] Gideon Schwarz. 1978. Estimating the Dimension of a Model. *The Annals of  
 296 Statistics* 6 (1978), 461–464.
- [8] Linda E. Strubbe and Eliot Quataert. 2009. Optical Flares from the Tidal Disruption  
 297 of Stars by Massive Black Holes. *Monthly Notices of the Royal Astronomical Society*  
 298 400 (2009), 2070–2084.
- 301
- 302
- 303
- 304
- 305
- 306
- 307
- 308
- 309
- 310
- 311
- 312
- 313
- 314
- 315
- 316
- 317
- 318
- 319
- 320
- 321
- 322
- 323
- 324
- 325
- 326
- 327
- 328
- 329
- 330
- 331
- 332
- 333
- 334
- 335
- 336
- 337
- 338
- 339
- 340
- 341
- 342
- 343
- 344
- 345
- 346
- 347
- 348